Scanning Microscopy

Volume 6 | Number 1 Article 12

2-6-1992

Simulating Ion Microtomography Data for Improving Reconstruction Quality

A. J. Antolak
Sandia National Laboratories

A. E. Pontau
Sandia National Laboratories

Follow this and additional works at: https://digitalcommons.usu.edu/microscopy

Part of the Biology Commons

Recommended Citation
Antolak, A. J. and Pontau, A. E. (1992) "Simulating Ion Microtomography Data for Improving Reconstruction Quality," *Scanning Microscopy*: Vol. 6 : No. 1 , Article 12.
Available at: https://digitalcommons.usu.edu/microscopy/vol6/iss1/12

This Article is brought to you for free and open access by the Western Dairy Center at DigitalCommons@USU. It has been accepted for inclusion in Scanning Microscopy by an authorized administrator of DigitalCommons@USU. For more information, please contact digitalcommons@usu.edu.

UtahStateUniversity
MERRILL-CAZIER LIBRARY

Scanning Microscopy, Vol. 6, No. 1, 1992 (Pages 157-166)
Scanning Microscopy International, Chicago (AMF O'Hare), IL 60666 USA

0891-7035/92$5.00+.00

SIMULATING ION MICROTOMOGRAPHY DATA FOR IMPROVING RECONSTRUCTION QUALITY

A. J. Antolak* and A. E. Pontau

Sandia National Laboratories
Livermore, CA 94551-0969

(Received for publication May 6, 1991, and in revised form February 6, 1992)

Abstract

Ion Microtomography (IMT) provides quantitative, fine resolution density imaging of samples for materials characterization. Reconstructed tomographic images are obtained by application of a filtered backprojection algorithm to the collected data. The attainable resolution and data acquisition rate are affected by several parameters. These include the number of ions measured per spot, using either the mean or median residual energy, utilizing Bragg additivity, changing the number of rays or the number of projections and oversampling the data. A tomography simulation computer program is described and used to study the contributions from these effects on the numerical reconstruction of an array of silicon pillars.

Key Words: Ion Microtomography, nuclear microprobe, materials characterization, proton microanalysis, image reconstruction, simulation code, tomography, reconstruction errors.

*Address for correspondence:
Arlyn J. Antolak
Theoretical Division 8341
Sandia National Laboratories
Livermore, CA 94551-0969 USA
Telephone: 510-294-3363
FAX: 510-294-3231

Introduction

The Ion Microtomography (IMT) technique is based on the energy lost by ions as they interact with the electrons in a sample [12]. A set of rotations (projections) and translations (rays) provides the data base for reconstructing a density image of the sample. A single projection consists of measuring the residual ion energy as a function of position as the focused ion beam is scanned across the sample. Numerous projections are acquired until the sample is rotated 360 degrees. For each projection, the measured residual energies are converted to line-integrated material densities using tabulated stopping powers [1]. The total (number of projections times number of rays) data set is mapped back into individual volumetric density elements using a filtered backprojection algorithm [9]. The result is a quantitative, three-dimensional map of the density variation within the sample.

The practicality of using IMT depends upon the attainable spatial resolution and the data acquisition rate [13]. Several parameters can affect the results. For example, increasing the number of residual ion energies measured per ray improves the statistics for determining the density, but also decreases the data acquisition rate. Since the energy spectra are slightly skewed distributions, the median energy is typically used in the measurements [11, 13]. However, standard numerical algorithms for obtaining the median are slower than the routines which compute the mean. This reduction in data analysis speed can be a limiting factor for large data sets. The median also reduces the deleterious effects of spurious noise in the data especially for low counts per ray. Noise reduces the ability to distinguish fine spatial features in the sample, e.g., edge

definition. The reconstruction quality is also affected by the conversion of the measured residual ion energy to a line-integrated density. Usually the average composition of a sample is known, but the internal distribution of elements is not. Thus an average stopping power, weighted according to Bragg additivity, is used in the conversion. At present, no reconstruction codes are capable of compensating for this effect directly.

Other variations in the density resolution can arise depending on the number of projections (or rays) used in the measurements. Because of the statistical nature of the scattering process, deconvoluting the experimental data into the individual contributions from the above parameters is difficult (or impossible). In this paper, an IMT data simulation code is described which allows the study of these parameters and how they influence the quality of the tomographic reconstruction. One advantage is that exact thicknesses (densities) can also be evaluated so error estimates of the attainable resolution are possible. Subsequent sections present the numerical scheme used to simulate the tomographic data for an array of silicon pillars and the analysis of reconstruction quality.

Simulation Model

Recently, IMT measurements were conducted on an array of silicon pillars with a 2 μm square 7 MeV proton beam [14]. The array consists of four 100 μm square pillars equally separated from each other by a 25 μm gap. This sample provides an ideal geometry for numerical simulation because small measured density variations are observable and the simulation routines are fairly straightforward to program. The numerical algorithm follows a data aquisition scheme analogous to the measurements. A set of projections consisting of line-integrated density rays are computed and stored in a data file. Then the filtered backprojection of the line-integrated density file yields the reconstructed density image of one slice through the silicon array. Numerous slices can be assembled to create a rendered three-dimensional image of the sample.

In the following analysis, the pillar array geometric space is partitioned into rotational and translational domains. The translational domain is subdivided into N equally spaced subintervals (steps) which extend beyond the longest extent of the sample ($225\sqrt{2}$ μm for the pillar array). In the simplest case, the translational step size is equal to the beam size. The rotational domain is also divided into M angular subintervals (projections). The trajectories of a fixed number of ions, K, are followed through the sample. Within a step, the spatial position of each ion is randomly sampled and the target thickness at that location is computed for the ion. The thickness, T, is obtained by superposing the intersections of the ion's trajectory and any pillars encountered. Each pillar in the array can be described mathematically by a set of linear trigonometric equations (see Ref. 3). The energy loss associated with a thickness is determined with the stopping power. Because ion scattering is stochastic in nature, the residual energy computed from the energy loss is mathematically broadened. The ion's residual energy is then sampled from the resulting energy spectrum. The energy loss associated with the sampled transmitted ion energy is again converted back to thickness with the inverse of the stopping power. This process leads to a distribution of material thicknesses for the K ions in the step. Finally, the single thickness assigned to the step is computed from the mean or median of the thickness distribution. Unless otherwise noted, the values for K, M, N, etc. in Table 1 are used in the simulations below.

Number of Ions Per Ray

As discussed in Ref. 14, a 7 MeV proton beam incident on 200 μm of silicon would require approximately K = 500 protons per ray to give a 0.2 μm thickness measurement; about K = 40 protons per ray are needed for the same density uncertainty through 2 μm. The difference in the counting statistics is primarily due to energy broadening (straggling) in the

Table 1. Parameters used in the Ion Microtomography (IMT) analysis of a silicon pillar array [13].

Experimental Parameter	Value
Beam Size	2 μm
Beam Energy	7 MeV
M (projections)	393
N (rays/projection)	250
K (ions/ray)	100
Sample Rotation	360°
Reconstruction Filter	Hamming (.45π cutoff)

thicker parts of the sample. The usual data acquisition scheme uses a fixed number of ions/ray for the entire sample. However, it is more advantageous to vary the number of collected ions so that more (less) ions are counted in thick (thin) regions. An additional benefit is the increased data acquisition rate.

Table 2 gives the average density in the pillars after reconstructing simulated data using the median of 40, 100, 500 and a varying number of protons/ray. In the latter case, the

Table 2. Mean and standard deviation silicon pillar densities for reconstructions with different numbers of ions per ray.

K (protons/ray)	Silicon Pillar Density (g/cm^3)
40	2.326 ± 0.029
100	2.327 ± 0.015
500	2.327 ± 0.010
varying	2.327 ± 0.011

number of ions sampled per ray is computed from K = 1.5 T + 35 where T is silicon thickness in microns. Thus, K varies from a minimum of 35 ($T \approx 0$) to 512 ($T = 225\sqrt{2}$) with an "equivalent" average value of 275. The conversion of silicon thickness to (from) an associated energy loss is made using tabulated stopping powers [1]. Each ion's energy is sampled from a Gaussian distribution broadened by the Bohr theoretical value [10]. As seen in the table, varying the number of ions per ray based on thickness yields results comparable to using a large, fixed number (K = 500) of counts per ray and, further, in this case, produces a reduced beam charge of 55%. Thus, the same level of resolution is attained at a faster rate, but determination of the thickness *a priori* in order to vary the count rate may be difficult to achieve experimentally. The increased efficiency is most important for large data sets as the beam size is reduced or the density resolution requirements are increased.

Mean vs. Median Residual Energy

According to the theoretical analysis of energy straggling, the energy loss domain can be roughly separated into three regimes. For very thin absorbers (e.g., rays near corners of the sample), the energy loss is dominated by infrequent single collisions with large energy transfers. This leads to a Landau-type distribution function [8]. Somewhat thicker absorbers yield Gaussian-shaped energy loss distributions described by the Bohr model [10]. Finally, large energy losses in thick regions depend upon the stopping power as a function of energy and result in skewed distributions given by Tschalär [15, 16]. For example, the 7 MeV proton beam used in the experiment loses about 4.5 MeV after passing through the diagonal of the silicon pillar array. The mathematical model used to sample these distributions for the energy loss is described in the appendix.

Besides straggling, the measured residual spectra can also contain noise which affects the energy loss and density values used in the reconstruction. The two principally observed sources of extraneous noise in the measured residual energy spectra are pulse pileup and slit scattering. Approximately 1% of the IMT spectral data is observed to be noise from these effects so, in the simulation, one randomly-selected proton out of every hundred is counted as a spurious event. Additionally, the 50-50 choice of whether the event is due to pulse pileup or slit scattering is also determined randomly. Pulse pileup is simulated by doubling the computed mean transmitted energy of the ion. If the resultant energy is greater than the incident energy (7 MeV), the particle is not counted. Noise resulting from slit scattering is modeled by halving the computed residual energy.

Initially, a simulation is made which addresses the case with no extraneous events; following this example is the case which includes both straggling and noise in the transmitted energy spectra. The results of determining the density in the central areas of the pillars is presented in Table 3 for the cases with and without spurious noise. If only energy straggling limits the resolution, there is slightly less variation in the density using the mean value of each residual energy spectrum. However, when 1% noise fluctuations are included in the spectral data, the median provides much better density resolution (approximately a factor of three). Similar results have been reported for the spatial resolution, e.g., edge definition, in the complementary technique of scanning transmission ion microscopy (STIM) [11]. The mean, on the other hand, yields lower pillar density values with noise because pulse pileup events leading to energies greater than the incident ion energy are not counted. In the

Table 3. Silicon pillar densities and standard deviations for reconstructions with energy broadening (straggling) with and without spurious noise included in the simulation. A comparison is made between using the mean or median values of the transmitted ion energy spectra during the data acquisition.

Energy Broadening	K	Pillar Density (g/cm^3) Mean Energies	Pillar Density (g/cm^3) Median Energies
Without noise	11	2.335±0.038	2.334±0.044
With noise	11	2.327±0.151	2.333±0.047
Without noise	100	2.334±0.013	2.333±0.016
With noise	100	2.326±0.049	2.332±0.017

cases with noise it can be seen that the density determined with the median of 11 ions/ray has variation equivalent to the one using the mean of 100 ions/ray.

Bragg Additivity

As pointed out earlier, the conversion from residual energy to line-integrated density affects the attainable density resolution. To study this, simulated ion tomography results are presented for an inhomogeneous sample. The same silicon pillar array as before is used except one pillar's composition is changed to gold. Since the stopping power curves for silicon and gold are different nonlinear functions of energy, the energy loss of an ion passing through gold followed by silicon will be different from the case had the ion traveled in the reverse direction. In the simulation, the total ion path is broken into segments ordered according to the silicon or gold thicknesses encountered. The energy loss in a segment is determined by numerically integrating the appropriate elemental stopping power. The residual energy calculated in one segment becomes the incident energy for the next and so forth. Finally, analogous to the IMT measurements, the resultant total energy loss is converted to a line-integrated electron density by numerically inverting an average stopping power for the sample derived from Bragg additivity. The simulation shows the mean and standard deviation density of the reconstructed volume elements located in the central areas of the pillars to be 3.352 ± 0.303 g/cm^3 for silicon and 18.296 ± 3.952 g/cm^3 for gold. Thus, the averaging effect of Bragg additivity has introduced a 44% increase in the actual silicon density (ρ = 2.33 g/cm^3) and a smaller (5%), but substantial, decrease in the gold density (ρ = 19.32 g/cm^3). Note, however, that the selected materials have extremely different stopping powers and were chosen to emphasize this effect. In some cases it may be possible to circumvent this error if the initial distribution of elements is (at least partially) known and the reconstruction codes are modified to take the additional information into account.

Number of Rays or Projections

Based on Huesman's analysis, [7] the number of projections, M, needed to minimize statistical errors in a reconstructed image must be at least $\pi L/2\Delta s$ where L is the maximum linear dimension of the sample (= $225\sqrt{2}$ µm for the pillar array) and Δs is the step (pixel) size. The corresponding number of rays per projection, N, is chosen to be at least $L/\Delta s$. This implies $M \geq 250$ and $N \geq 160$ for the 2 µm square beam used in the measurements. The effect of decreasing the number of rays (or projections) is studied in the following manner. To avoid the approximations made by converting to energy loss with the stopping power, only the exact target thicknesses corresponding to each of the K = 100 ions/step are determined. The median of the resulting thickness distribution is then expressed as a line-integrated areal density (g/cm^2) by multiplying by the density of silicon. In the simulation, first the number of rays, N, is sequentially decreased for a fixed number of projections, M, and then the number of projections is decreased for fixed N. Table 4 displays the mean and standard deviation density of the reconstructed volume elements within the silicon pillars. The results indicate that the reconstruction quality is slightly more sensitive to a decrease in the number of projections rather than the number of rays. On the other hand, as the value of M or N gets larger, there is a point of diminishing returns where the resolution can only be improved by increasing K. These results are consistent with a similar analysis performed on the experimental data of Ref. 14.

Oversampling

In principle, a large beam can detect small density variations if the beam is translated in steps comparable to (or smaller than) the beam size. The density information each ray carries in this case is the superposition of data obtained from the beam overlapping neighboring steps. Figure 1 shows the reconstructed images from the simulated IMT data for a fixed Δs = 2 µm step and beam

Table 4. Mean and standard deviation silicon pillar densities for reconstructions with varying numbers of projections or rays.

M (projections)	N (rays/projection)	Silicon Pillar Density (g/cm^3)
393	25	2.009 ± 0.497
393	50	2.310 ± 0.025
393	100	2.331 ± 0.015
393	150	2.328 ± 0.015
393	200	2.327 ± 0.015
51	250	2.324 ± 0.088
75	250	2.320 ± 0.052
101	250	2.328 ± 0.036
151	250	2.327 ± 0.020
201	250	2.327 ± 0.016

dimension increasing in size from 2 to 8 μm. Similar to the previous section, only exact areal densities are computed in each step and their median value is assigned to a ray. Also shown in the figure are the mean and standard deviation density from a region within the central area of the pillars, and a plot of density versus position for a line scan across the lower two pillars. As expected, for a fixed number of ions per ray, some degradation in reconstruction quality occurs as the beam size increases but features significantly smaller than the beam size can be resolved, e.g., edge and corner definition.

Summary

In typical ion microtomography (IMT) applications there are tradeoffs between the attainable resolution and the data acquisition and analysis rates. Depending on the specimen and what is to be studied, it is generally better to try to minimize the number of steps required to give the desired information without sacrificing image quality. In this work, a simulation code is described for studying reconstruction quality in IMT measurements. The code is a useful tool in establishing error

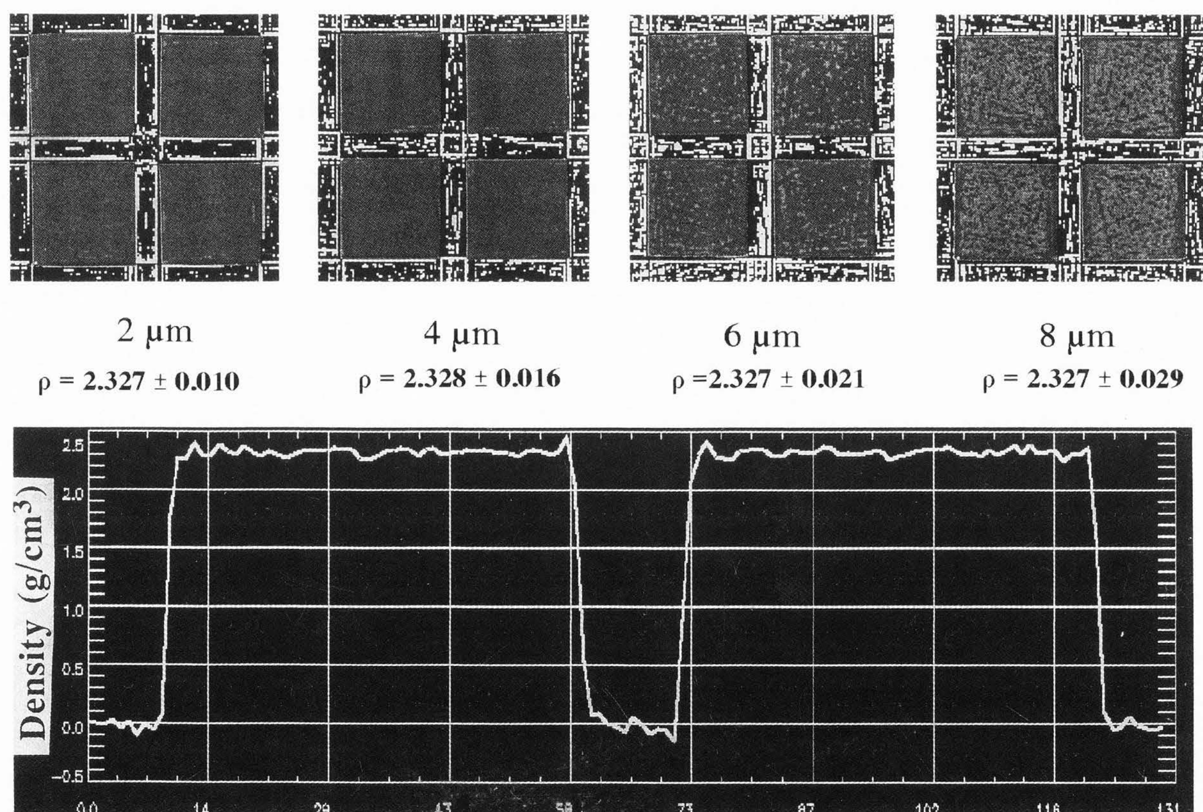

Fig. 1 Reconstructed images from simulated ion microtomography data for the silicon pillar array using progressively larger beam sizes and a fixed step size of 2-μm. The top row displays the results for 2, 4, 6 and 8-μm beam sizes with the mean and standard deviation density given for a region within the central areas of the pillars. The lower plot is a line density scan across the bottom two pillars of the 8-μm beam image.

estimates of the attainable resolution from various experimental and reconstruction parameters. Knowledge of the relative contributions of these errors allows for refinements to be implemented in the experiment which improve data acquisition and analysis rates. For example, varying the number of ions per ray depending on the sample thickness yields results comparable to a large, fixed number of ions/ray. The resolution quality is preserved with faster data acquisition time. Although median algorithms are slower computationally than those for the mean, much better density resolution is obtained in the reconstructed image if noise in the residual energy data exists. Future reconstruction codes need to be modified so that *a priori* information can be utilized to minimize the effects of Bragg additivity. It also appears that the reconstruction algorithms are somewhat more sensitive to using fewer projections rather than fewer rays. Using steps smaller than the beam size makes it possible to discern fine spatial features without having to produce even smaller microbeams. Balancing these factors in IMT will lead to better reconstruction quality in the final images.

Appendix

Sampling the energy loss distributions in the simulation results in a substantial increase in computational time. Of the three types of distributions, only one is expressible in a simple analytic form, i.e., Gaussian with Bohr width. In this case, the energy loss can be sampled directly in the code. Bohr theory is used when the relative energy loss, $\Delta E/E_o$, is between 0.05 and 0.25. Here ΔE is the average energy loss determined from the stopping power for silicon and E_o is the incident energy [6]. For the remaining two distributions, efficient sampling is accomplished by following a procedure similar to the one described in Ref. 2, but modified for 7 MeV proton scattering in silicon. The Landau distribution is used when $\Delta E/E_o < 0.05$ [8]. Following Ref. 2, the non-dimensional variable λ in the Landau distribution is obtained from:

$$\lambda = \begin{cases} 1.92 \sin^{-1}(2.77R-1)-0.257, & R<0.674 \\ -3.23 \ln(1.774-1.7729R), & R\geq 0.674 \end{cases} \quad (1)$$

where R is a random number. The sampled energy loss, ΔE^* (MeV), corresponding to the above λ is computed from:

$$\Delta E^* = 0.00121\, T\,\{\lambda + \ln(929\, T)\} \quad (2)$$

for silicon of thickness T microns. When $\Delta E/E_o > 0.25$, the same sampling procedure as above is applied except that the functions in Ref. 2 are fit to Tschalär's energy loss distributions for the bulk region [15]. From his figures, the full width at half maximum, Γ, of each distribution is given approximately by:

$$\Gamma = 2.19 - 0.000545\,(1-\Delta E/E_o)^{-2.96} \quad (3)$$

The integrals I_1 and I_2 in Ref. 2 for 7 MeV protons in silicon are:

$$I_1 = 0.891\,\Gamma \quad \text{and} \quad I_2 = \frac{\kappa}{\beta}\,(e^{-\beta\Gamma/2} - e^{-5\beta}) \quad (4)$$

where:

$$\kappa = 0.19\, e^{1.23\Gamma} \quad \text{and} \quad \beta = 0.412 + 0.466\,\Gamma \quad (5)$$

In his paper, Tschalär plots the bulk region energy loss distributions as a function of $\tau = (E_m - E)/\sigma$ where E_m is the modal, not mean, transmitted energy and σ is the standard deviation of the residual energy spectrum. In a subsequent paper [16], he showed that the modal energy differs from the mean value by only about 0.5-3.0% in the bulk region. Following Ref. 2, the value of τ is sampled from:

$$\tau = \begin{cases} \frac{3\Gamma}{2\pi}\sin^{-1}\left[\frac{2\pi}{3\Gamma}(I_1+I_2)R - 1\right], & R<\frac{I_1}{I_1+I_2} \\ -\frac{1}{\beta}\ln\left[e^{-\beta\sigma/2} - \frac{\beta}{\kappa}\{(I_1+I_2)R - I_1\}\right], & \text{otherwise} \end{cases} \quad (6)$$

for a random number R. Assuming $\Delta E \approx \Delta E_m$, the sampled energy loss, ΔE^* (MeV), is computed from:

$$\Delta E^* = \Delta E + \sigma\,\tau \quad (7)$$

where an energy-dependent empirical

expression is used to evaluate σ [4, 5]. The advantage of the above procedure is that analytically integrable and invertible functions are used so direct sampling of the energy loss is possible.

Acknowledgements

This work was supported by the U.S. Department of Energy under contract No. DE-AC04-76P00789. The authors wish to thank D.L. Weirup and D.H. Morse for helpful assistance.

References

[1]Andersen HH, Ziegler JF (1977) *Hydrogen Stopping Powers and Ranges in All Elements*. Pergamon, New York, 16-25.

[2]Antolak AJ, Williamson, Jr. W (1990) "A semiempirical nonrelativistic electron straggling distribution function" J. Appl. Phys. **67** (3) 1510-1514.

[3]Antolak AJ and Pontau AE (1991) "On data reduction errors in proton energy loss measurements" Nucl. Instr. Meth. **B54**, 371-377.

[4]Antolak AJ, Handy BN, Morse DH, Pontau AE (1991) "Energy loss and straggling measurements of ions in solid absorbers" Nucl. Instr. Meth. **B59/60** 13-17.

[5]Bauer GH, Antolak AJ, Pontau AE, Morse DH, Heikkinen DW, Proctor ID (1989) "Proton energy straggling measurements in aluminum, titanium, silver and tungsten foils" Nucl. Instr. Meth. **B43** 497-501.

[6]Besenbacher F, Andersen JU, Bonderup E (1980) "Straggling in energy loss of energetic hydrogen and helium ions" Nucl. Instr. Meth. **168** 1-15.

[7]Huesman RH (1977) "The effects of a finite number of projection angles and finite lateral sampling of projections on the propagation of statistical errors in transverse section reconstruction" Phys. Med. Biol. **22** 511-521.

[8]Landau L (1944) "On the energy loss of fast particles by ionization" J. Phys. (USSR) **8** (4) 201-205.

[9]Martz HE, Azevedo SG, Brase JM, Waltjen KE, Schneberk DJ (1991) "Computed tomography systems and their industrial applications" Int. J. Rad. Appl. and Instr. **41** (10/11) 943-948.

[10]Mayer JW, Rimini E (1977) *Ion Beam Handbook for Material Analysis*. Academic Press, New York, 1-20.

[11]Overley JC, Schofield RMS, MacDonald JD, Lefevre HW (1988) "Energy-loss formation in scanning transmission ion microscopy" Nucl. Instr. Meth. **B30** 377-382.

[12]Pontau AE, Antolak AJ, Morse DH, Ver Berkmoes AA, Brase JM, Heikkinen DW, Martz HE, Proctor ID (1989) "Ion microbeam tomography" Nucl. Instr. Meth. **B40/41** 646-650.

[13]Pontau AE, Antolak AJ, Morse DH (1990) "Some practical considerations for ion microtomography" Nucl. Instr. Meth. **B45** 503-507.

[14]Pontau AE, Antolak AJ, Morse DH, Weirup DL (1991) "Minimum data set requirements for ion microtomography" Nucl. Instr. Meth. **B54**, 383-389.

[15]Tschalär C (1968) "Straggling distributions of large energy losses" Nucl. Instr. Meth. **61** 141-156

[16]Tschalär C (1968) "Straggling distributions of extremely large energy losses" Nucl. Instr. Meth. **64** 237-243.

Discussion with Reviewers

S. Tapper: In the paper, it is stated that IMT is a quantitative method. In a later section, it is shown that introducing gold in part of the sample matrix results in a 44% error in the density determination of silicon. Couldn't a contamination, or a cavity, in an unknown sample also give a similar effect, i.e., you must assume the true sample (which is what you measure) if the correct density with standard deviation is to be given?

P. Spanne: This paper describes a simulation program that is used to assess the uncertainties involved in ion microtomography reconstructions. Such a program seems to be a prerequisite for ion microtomography rather than a onetime tool for evaluation of general parameters for ion tomography. This is so because there does not exist any unambiguous solution to the problem of finding the line integrals of the density from energy loss measurements in samples containing several elements. This ambiguity arises from the dependence of the stopping power on both the material and the ion energy. The authors state that this is of concern and show that the errors can be considerable, as is the case for the gold-silicon sample. Although this sample is

considered to be a kind of worst case, it is not explained why it is so. In general, I consider this problem of much concern and want to encourage the investigators to extend their work on this.

B.L. Doyle: This is a very specialized paper concerning the optimization of ion microtomography using computer-simulated tomographs. In the section on Bragg Additivity, it was pointed out that a 44% error in Si density results due to the non-linear dependence of stopping power on beam energy when non-homogeneous samples are examined. I really don't understand the source of this error: do back-projection methods assume that the stopping powers are linear functions of energy? This seems to be the most striking difference between conventional CT (computed tomography) scans and IMT, and I would be very interested to have some added discussion comparing the two (i.e., CT-IMT) on this point. It would seem that such a problem must be resolved before IMT can reach its full potential.

Authors: In our analysis we "assume" the specimen is of uniform elemental composition and that any ion energy loss is directly due to the electron density of the material. Voids, density changes, and the spatial extent of the specimen are determined directly and quantitatively for materials of uniform composition. The absolute accuracy of the measurements is related to the accuracy of tabulated stopping powers and Bragg's Rule.

As indicated in the text, *composition* variations are not treated in the basic reconstruction process. They result in inaccurate density calculations because for any particular ray through the specimen, the *wrong* (composite) stopping power is used instead of the locally correct one. For specimens with relatively simple internal structures of known composition, we could conduct an iterative process to increase reconstruction accuracy.

S. Tapper: What are the advantages and disadvantages with IMT when compared with synchrotron X-ray microtomography?

Authors: IMT has a number of advantages over synchrotron X-ray microtomography. For example, low atomic number elements are not masked by high Z elements, no beam hardening effects are present, no beam intensity normalization is required, beam brightness is not an issue, and the target potentially receives lower radiation damage. The limitations of IMT are the range of the ions (which limits the specimen size), the amount of spatial broadening (which limits the attainable resolution), and the data acquisition rates (which limit its use as a production tool).

G.J.F. Legge: You do not mention the effect of scattering (also a statistical process) on spatial resolution; but you say that the trajectories of the ions are followed through the sample. Have you included angular straggling (beam scatter) effects?

H.W. Lefevre: Your simulation ignores small angle scattering of protons as they penetrate the specimen, and the attendant loss of spatial resolution with energy loss. This effect also will set a limit beyond which increasing the number of ions per ray or smaller beam sizes will not improve resolution or accuracy in the density reconstruction. If this effect is not included, your simulation can overestimate the accuracy and resolution that can be achieved. It can also suggest that a larger number of ions per ray will improve the reconstruction while actually it won't. For the case of your silicon pillars, have you investigated the effect of small angle scattering? If so, for what number of ions per ray at the smallest beam size is it the dominant effect?

Authors: The ultimate resolution attained with IMT may be limited by the spatial broadening of the beam. However, the issues relating to beam scatter on the quality of the reconstructions are beyond the scope of this paper. We are conducting an analysis of small angle scattering which will be presented in a future paper.

G.J.F. Legge: In regard to oversampling, the median provides better edge definition than the mean, but only the mean could resolve internal structure (such as a dense sphere or a hole) smaller than the beam size. Such structures would be equivalent to noise, which the median ignores. Do you have any evidence or comment on this matter?

Authors: The median does not ignore noise, but, instead, filters out extreme data thereby giving a more representative measure of central tendency for skewed or noisy distributions. Also, the mean can not *resolve* an internal structure smaller than the beam size, but it could be distinguished. We have compared simulations with exact thicknesses using the mean and median energy loss for such a case. Provided there is no noise, the median fails to detect features smaller than the

beam size. On the other hand, the median energy loss is used in the measurements because spurious counts always occur during data acquisition.

H.W. Lefevre: You find that 1% noise introduced into the simulation markedly affects the density resolution when means rather than medians of energy losses are used. Yet your modeling of the noise itself appears to be rather casual. Have you compared a measured noise distribution with that used in your simulation? Shouldn't you include the (almost) full energy events which occur when slit scattering barely degrades the energy of a proton but causes the proton to miss the specimen completely?
Authors: The noise model used in the simulation is rather simplistic and most likely does not completely represent the experimental situation. As you have pointed out, there are other contributions to the noise. However, the model does serve to illustrate the differences between using the median versus the mean energy loss when spurious events occur in the data without the necessity of introducing excessive complexity into the analysis.

H.W. Lefevre: Lefevre *et al.* [Lefevre HW, Schofield RMS, Bench GS, Legge GJF (1991) Nucl. Instr. Meth. **B54**, 363] have shown that the absolute uncertainty in areal density first increases with energy loss and then decreases. They also showed that the fractional uncertainty in areal density decreases monotonically with increasing energy loss despite the fact the energy spread increases. Why, then, don't you simulate using more protons in areas where the areal density is most uncertain rather than, as you do, using more protons where the energy straggling is largest?
Authors: The basic reconstruction problem is the assignment of mass to individual volume elements within the analyzed region. Thus, it is our opinion that the relevant figure of merit for IMT analysis is the *absolute* uncertainty in areal density, σ_{AD}, rather than the *relative* uncertainty for particular rays. In fig. 2, we have plotted this calculated parameter in terms of areal density straggling versus total energy loss for 7 MeV protons incident on silicon. Here, we have used our straggling formula from Bauer *et al.* rather than Bohr straggling which *underestimates* straggling for high

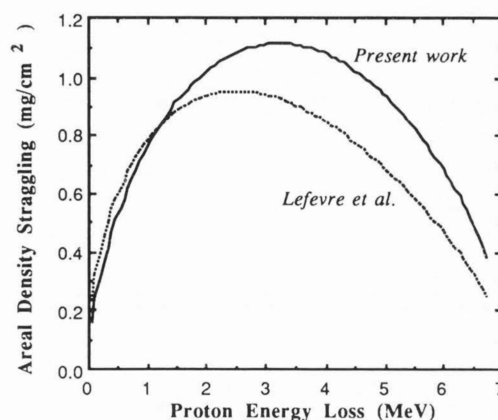

Fig. 2. Areal density straggling vs energy loss for 7 MeV protons slowing down in silicon. The Lefevre *et al.* curve uses Bohr theory to determine the standard deviation in energy loss; the present work computes the energy loss standard deviation according to the empirical formula of Bauer *et al.*

relative energy loss [5]. (Our formula may still also underestimate straggling for E/E_0 greater than about 0.8 [15, 16]).

For the analysis in this paper we have used the simplification of a linear increase in number of ions used relative to the thickness of the specimen. The results of using this method clearly demonstrate the advantage of varying the number of protons used with sample thickness. We note that for 7 MeV protons incident on the silicon specimen modeled, the maximum energy loss is about 4 MeV.

A more rigorous approach would assign the number of ions used, K, by equalizing the absolute areal density uncertainty, σ_{AD}, for all rays through the specimen. (σ_{AD} should encompass all contributions to areal density uncertainty including instrumental energy broadening.) We can choose K_σ by allowing it to vary proportionally to $(\sigma_{AD})^{1/2}$. We have plotted the portion of K_σ due to energy straggling versus specimen thickness in fig. 3 for comparison with the K we used for the illustration.

In the future, we expect to incorporate K_σ in our data acquisition scheme by conducting a cursory IMT scan of the specimen to establish approximate median energy losses and standard deviations, and adjust our acquisition parameters accordingly.

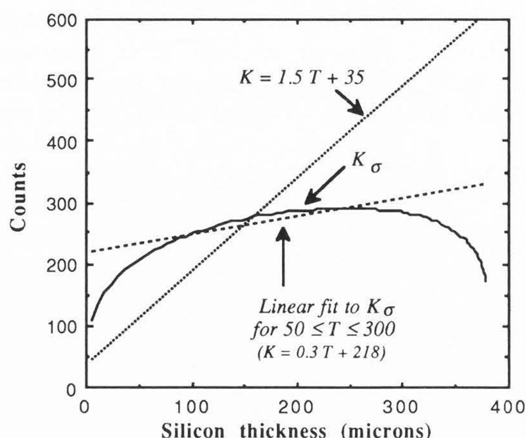

Fig. 3. Comparison of functions used to vary the number of ion counts per ray with changing silicon thickness for 7 MeV protons. K_σ corresponds to the case when the number of ions used in each ray equalizes the absolute density uncertainty for all rays through the specimen. The approximation K = 1.5*T+35 used in the present work underestimates (overestimates) the required number of counts in thin (thick) regions, but has the same qualitative trends as K_σ. An improved linear approximation is also shown for illustrative purposes, but better agreement would require nonlinear fitting functions.

M. Breese: All the work I have seen published on IMT has considered very simple samples, such as glass tubes. If IMT is to become a genuinely useful analytical technique, it must have "real" applications. What applications in materials characterization do you envision for IMT?

Authors: In energy sciences, we are using IMT to characterize the uniformity and sphericity of direct drive inertial confinement fusion targets and have proposed its use in verifying the integrity of carbon coatings on fission fuel pellets in next-generation nuclear energy reactors. In biological sciences, IMT can be used at the subcellular level to establish, for example, the distribution of polyanions used to inhibit replication of the HIV virus and to distinguish morphologically similar structures such as the Alzheimer plaques which surround brain tissue. Full three-dimensional characterization of microcircuits and flaw or defect detection in materials are additional areas we are exploring.

M. Breese: Would it be possible to be more quantitative in calculating how small or thin a feature can be imaged with a given beam resolution and stopping power for a fixed number of incident protons?

Authors: Unfortunately, the reconstruction process convolves so many different factors that it will be difficult to derive universal expressions for spatial resolution and density sensitivity. Since energy straggling, stopping power, and spatial broadening are functions of both beam energy and specimen composition, they must be included parametrically. We have not yet incorporated spatial broadening of the beam into the reconstruction process, nor have we investigated sufficiently the effects of the various filters available. The reconstruction process itself also introduces noise into images as we have discussed in earlier papers [3, 12-14].